



Ni-Co-Mo-O nanosheets decorated with NiCo nanoparticles as advanced electrocatalysts for highly efficient hydrogen evolution

Shuaiwei Wen^a, Tao Yang^a, Naiqin Zhao^{a,b}, Liying Ma^a, Enzuo Liu^{a,b,*}



^a School of Materials Science and Engineering and Tianjin Key Laboratory of Composites and Functional Materials, Tianjin University, Tianjin, 300350, China

^b Collaborative Innovation Centre of Chemical Science and Engineering, Tianjin, 300072, China

ARTICLE INFO

Keywords:

Ni-Co-Mo-O nanosheets
NiCo nanoparticles
Synergistic effect
Electrocatalyst
Hydrogen evolution reaction

ABSTRACT

The development of efficient and durable HER electrocatalysts is urgently required to enhance the efficiency of water splitting. Here we report the Ni-Co-Mo-O nanosheets decorated with NiCo nanoparticles supported on NF (NF/NiCoMoO-H₂) as efficient HER electrocatalysts in alkaline media. The introduction of oxygen vacancies and multiple metal ions (Ni-Co-Mo-O nanosheets) accelerates water dissociation, while metal atoms (NiCo nanoparticles) promote the adsorption and association of hydrogen intermediates into H₂ molecules. The efficiently synergistic effect between Ni-Co-Mo-O nanosheets and NiCo nanoparticles results in the NF/NiCoMoO-H₂ with a low overpotential of 15 mV at 10 mA cm⁻² and Tafel slope of 33.1 mV dec⁻¹. More importantly, the water-alkali electrolyzer using NF/NiCoMoO-H₂ as cathode and NF/NiFe-LDH as anode shows a low voltage of 1.44 V at 10 mA cm⁻² and remarkable stability. Owing to the controllable fabrication process and excellent HER performance, the NF/NiCoMoO-H₂ is a promising electrocatalyst for the practical water splitting.

1. Introduction

Hydrogen is widely recognized as an ideal alternative fuel due to its cleanliness, high efficiency and renewability [1,2]. However, mass hydrogen production by electrocatalytic splitting of water has been limited by the sluggish HER (Hydrogen evolution reaction) kinetics and enormous electricity consumption [3,4]. Platinum (Pt) is the most effective and benchmark electrocatalyst for HER [5]. Unfortunately, the low abundance and high cost restrict its large-scale application [6]. It is crucial to develop low-cost, highly efficient, robust and highly active HER electrocatalysts for enabling high efficiency hydrogen production [7,8].

Until now, many non-precious-metal based materials, such as 3d transition metals (TMs) (e.g., Ni, Co, Fe, Mo, etc.) oxides, sulphides, carbides, nitrides and phosphides, and nonmetallic materials, have been widely studied as potential candidates for HER electrocatalysts [9–12]. Significant progress has been acquired under acidic conditions [13–15]. Nevertheless, under alkaline conditions, there is still a large gap between the current noble-metal-free electrocatalysts and the Pt-based electrocatalysts [16–18]. This phenomenon might be related to the different fundamental HER mechanisms on the surfaces of electrocatalysts in alkaline and acid solutions [19]. More specifically, the sluggish HER kinetics in alkaline solutions is mainly due to the fact that

H⁺ used for HER is mainly derived from water dissociation (Volmer step) rather than direct hydronium ions in the electrolyte [20–22]. Thus, accelerating the Volmer steps is important to develop high performance HER electrocatalysts [23]. Markovic et al. demonstrated that high valence metal ions in oxides or hydroxides can weaken the O–H bond of adsorbed water, promoting water dissociation [24]. Greeley et al. revealed that metallic atoms can provide an appropriate binding energy to stabilize adsorbed hydrogen, accelerating the formation of H₂ molecules [25]. Thus, combining single metal or metal alloys with metal oxides may be of great promise to prepare highly active HER electrocatalysts in alkaline electrolytes [26–30]. In 1994, Fan and his co-workers reported that Ni-Co-Mo-based catalyst exhibited superior HER performance in alkaline electrolytes compared with Ni, Co, Ni-Mo and Co-Mo [31]. In addition, owing to the inherent requirement of high electron transport and multiple active sites for HER electrocatalysts, electrical conductivity and structural design (such core/shell or porous structure) are also the key factors affecting the performance of the catalyst [32,33].

Herein, we propose a facile fabrication of the Ni-Co-Mo-O nanosheets decorated with NiCo nanoparticles supported on Ni foam (NF/NiCoMoO-H₂) using hydrothermal process and low-temperature hydrogenation process. The as-fabricated NF/NiCoMoO-H₂ electrocatalyst creates efficiently synergistic effect between Ni-Co-Mo-O nanosheets

* Corresponding author at: School of Materials Science and Engineering and Tianjin Key Laboratory of Composites and Functional Materials, Tianjin University, Tianjin, 300350, China.

E-mail address: ezliu@tju.edu.cn (E. Liu).

and NiCo nanoparticles. Furthermore, the NF/NiCoMoO-H₂ displays good electrical conductivity and high oxygen vacancies, accelerating the transfer of electrons and increasing the HER active sites. As a result, the NF/NiCoMoO-H₂ electrocatalyst exhibits excellent HER activity and superior long-term stability under alkaline conditions. Moreover, our home-made water electrolyzer achieves the top level of water electrolyzer reported up to date.

2. Experimental section

2.1. Synthesis of electrode material

Commercial Nickel foam (NF, 3 cm × 3 cm, Tianjin Aiweixin Ltd.) was cleaned ultrasonically in 3 M HCl (Tianjin Jiangtian Ltd.) for 20 min to remove the surface oxides and then washed with deionized water. Afterward, the clean NF was immersed into the 80 mL aqueous solution containing 0.726 g NaMoO₄·2H₂O (Tianjin Heowns LLC.) and 0.873 g Co(NO₃)₂·6H₂O (Tianjin Kermel Ltd.) in a Teflon-lined stainless autoclave (100 mL). The sealed autoclave was kept at 150 °C for 6 h. After the reaction was over, the product was washed and dried in a vacuum oven at room temperature to obtain NF/NiCoMoO-precursor. Then NiCo nanoparticles decorating on Ni-Co-Mo-O nanosheets on NF (NF/NiCoMoO-H₂) was obtained by calcining NF/NiCoMoO-precursor at 500 °C for 2 h in H₂/Ar (v/v, 20/180) reduction atmosphere with a heating rate of 2 °C min⁻¹. The mass loading of active material on the nickel foam calculated by the mass difference was about 2.7 mg cm⁻² (NF/NiCoMoO-H₂). All reagents were used as received without further treatment.

2.2. Preparation of NF/NiFe-LDH electrode

In brief, the above clean NF (2 cm × 3 cm) immersed into the 36 mL aqueous solution containing 0.202 g Fe(NO₃)₃·9H₂O (Tianjin Heowns LLC.) and 0.1454 g Ni(NO₃)₂·6H₂O (Alfa Aesar) in a Teflon-lined stainless autoclave (50 mL). The sealed autoclave was heated to 100 °C for 12 h. After the reaction was over, the product was washed and dried in a vacuum oven at room temperature to obtain NF/NiFe-LDH.

2.3. Structure characterizations

The morphology and microstructure were characterized by scanning electron microscope (SEM, Hitachi S4800) and transmission electron microscope (TEM, PhilipsTecnai G2 F20). X-ray diffraction (XRD) patterns were recorded on Bruker D8 Advanced with Cu K α radiation. The nitrogen adsorption isotherms of samples were measured at 77 K using an AutosorbIQ instrument (Quantachrome U.S.). XPS experiments were carried out on a PHI5000 VersaProbe.

2.4. Electrochemical measurements

All electrochemical tests were performed on a CHI760E electrochemical workstation at room temperature using a three-electrode system in 1 M KOH (Tianjin Kermel Ltd.) aqueous solution. The sample was examined directly as working electrode. A graphite rod and a saturated calomel electrode (SCE) were used as counter and reference electrodes, respectively. All polarization curves were measured by linear sweep voltammetry (LSV) at a scan rate of 5 mV s⁻¹ to evaluate the HER performance of the prepared samples. And the potentials can be converted to the potentials versus RHE by E(RHE) = E(SCE) + 0.241 + 0.059 pH. All the polarization curves were corrected for the iR compensation. Electrochemical impedance spectroscopy (EIS) was carried out with a frequency range from 0.01 Hz to 100 kHz, and the curve was fitted by Zview software. The electrochemically active surface area (ECSA) was estimated from the electrochemical double-layer capacitance of electrocatalysts. The double layer capacitance (C_{dl}) was determined with a simple cyclic voltammetry (CV) method at non-

faradaic potentials (0.2 ~ 0.3 V vs. RHE). The ECSA was then calculated by $ECSA = C_{dl}/C_s$. C_s is the specific capacitance of an atomically smooth planar surface with a real surface area of 1.0 cm², which is 20~60 μ F cm⁻² under alkaline media, and an average value of 40 μ F cm⁻² was used in this work.

For comparison, Pt/C (20 wt%, Shanghai Hensen Ltd.) and RuO₂ (99.9 wt%, Alfa) were loaded on NF. Their inks were prepared by mixing 6 mg catalyst with 960 mL ethanol and 40 mL Nafion solution (5 wt%) under sonication, and the mass loading onto the NF can be adjusted by controlling the amount of ink.

The water electrolysis was performed in a two-electrode system using the NF/NiCoMoO as the cathode and the NF/NF-LDH as the anode. For the purpose of comparison, the catalytic performance of NF/Pt/C//NF/RuO₂ for the water electrolysis was also tested under a similar condition. The linear sweep voltammetry curve was tested at a scan rate of 5 mV s⁻¹. And the polarization curves were given without the iR compensation.

3. Results and discussion

The NF/NiCoMoO-H₂ electrocatalyst was synthesized by a two-step process, as schematically illustrated in Fig. 1a. Firstly, the initial Ni-CoMoO-precursor nanosheets arrays grown on 3D Ni foam (NF/Ni-CoMoO-precursor) was prepared via a hydrothermal process using Ni foam itself as a Ni source, cobalt nitrate hexahydrate as a Co source and sodium molybdate dihydrate as a Mo source. Secondly, the Ni-Co-Mo-O nanosheets decorated with NiCo nanoparticles supported on NF (NF/NiCoMoO-H₂) was obtained by calcining NF/NiCoMoO-precursor in H₂/Ar atmosphere at 500 °C for 2 h. SEM images (Fig. 1b and c) of the NF/NiCoMoO-precursor demonstrate that a large number of nanosheets with smooth surface are uniformly grown vertically on the surface of NF skeleton. X-ray diffraction (XRD) analysis (Fig. S1) confirms that the NiCoMoO-precursor is a mixture of crystalline NiMoO₄·xH₂O (JCPDS No. 13-0128) and CoMoO₄·xH₂O (JCPDS No. 26-0477) [34]. After annealing in H₂/Ar atmosphere at 500 °C, the structure of nanosheets had no apparent change, but the surface of nanosheets became very rougher due to the presence of a large number of nanoparticles (Fig. 1d and e). According to the cross-section SEM image (Fig. 1f), it is further confirmed that these nanoparticles are evenly distributed on both surfaces of the nanosheets with the depth of ~500 nm. The XRD pattern of the NiCoMoO-H₂ in Fig. 1g shows that in addition to the three strong peaks of the NiCo alloy, the other peaks can correspond well to the phase of Co₂Mo₃O₈ and Ni₂Mo₃O₈ [20]. In contrast, the surface of the nanosheets through annealing in Ar atmosphere (NiCoMoO-Ar) is smooth (Fig. S2), and the composition of NiCoMoO-Ar nanosheets is NiMoO₄ and CoMoO₄ [35]. Therefore, the hydrogenation process is a key parameter for the formation of NiCo nanoparticles on Ni-Co-Mo-O nanosheets.

TEM image in Fig. 2a shows that the nanoparticles are dispersed on the surface of Ni-Co-Mo-O nanosheets with nanoporous structure. The nanoparticle size distribution histogram in Fig. S3 indicates that the NiCo nanoparticle size ranges from 4 to 40 nm, and the average size is 16.3 nm. The special surface area of porous NiCoMoO-H₂ nanosheets is 73.0 m² g⁻¹, and the pore size distribution is mainly around 4.2 nm (Fig. S4). High-resolution TEM (HRTEM) image (Fig. 2b) indicates that these nanoparticles exhibit high crystallinity with lattice spacing of 0.204 nm and 0.177 nm corresponding to (111) and (200) planes of NiCo alloy, respectively. And, the diffraction spots (the inset in Fig. 2b) obtained by Fourier transform are also indexed well to (111) and (200) planes of NiCo alloy, which is consistent with the XRD result. The HRTEM image also displays the lattice fringes of 0.242 and 0.221 nm corresponding to the (200) and (202) planes of Ni₂Mo₃O₈, respectively. Another lattice fringe with the distance of 0.249 nm corresponds well to (200) plane of Co₂Mo₃O₈. Scanning transmission electron microscopy (STEM) and the corresponding elemental mapping images reveal the uniform distribution of Mo and O throughout the whole surface of the

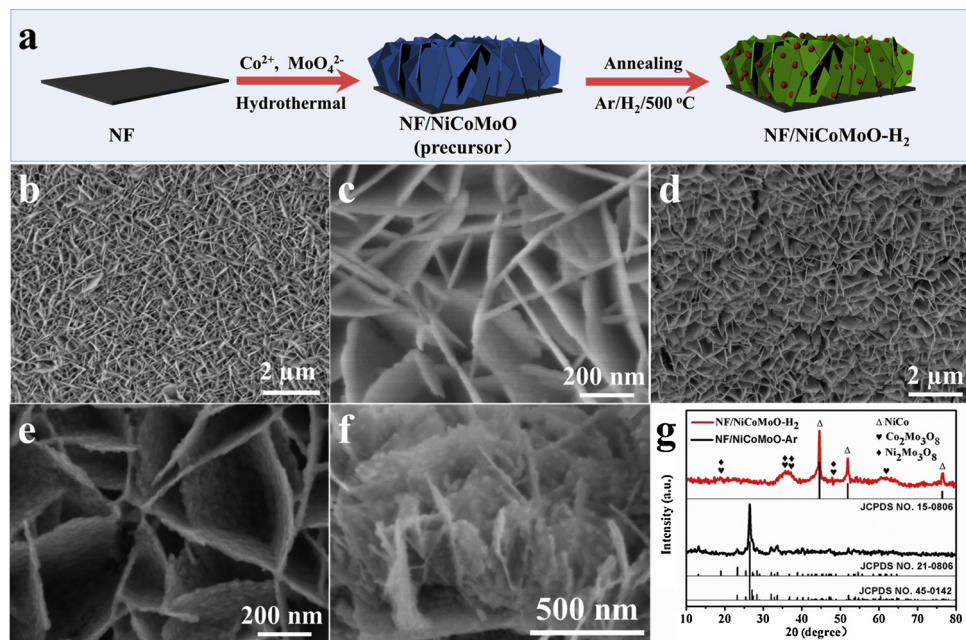


Fig. 1. (a) Schematic illustration of the preparation of the NF/NiCoMoO-H₂. (b, c) SEM images of NF/NiCoMoO-precursor. (d, e) SEM images of NF/NiCoMoO-H₂. (f) Cross-section SEM image of NF/NiCoMoO-H₂. (g) XRD patterns of NiCoMoO-H₂ and NiCoMoO-Ar.

nanosheets, while Ni and Co elements appear simultaneously in the distinguishable particle regions. Thus, the combined analysis of the above characterization on microstructure and spectrum confirms the prepared sample is Ni-Co-Mo-O nanosheets decorated with NiCo nanoparticles on the 3D NF substrate.

In order to evaluate the HER performance of catalysts, a typical three-electrode cell in 1 M KOH aqueous solution was used. The NF/NiCoMoO-H₂ was examined directly as working electrode. A graphite rod and a saturated calomel electrode (SCE) were used as counter and reference electrodes, respectively (Fig. S5) [36]. All polarization curves were measured by linear sweep voltammetry (LSV) at a scan rate of 5 mV s⁻¹. As presented in Fig. 3a, the pure NF shows a very poor HER activity, and the NF/NiCoMoO-Ar electrode exhibits an ordinary HER activity with an overpotential of 181 mV at 10 mA cm⁻². However, the HER onset potential of the NF/NiCoMoO-H₂ catalyst is close to that of the NF/Pt/C catalyst with the same mass loading, suggesting its excellent HER activity. The Fig. 3b shows that the NF/NiCoMoO-H₂ catalyst requires an extremely low overpotential of 15 mV at a benchmark current density of 10 mA cm⁻², and only 39 mV at 50 mA cm⁻², which

is close to the values of NF/Pt/C catalyst (5 mV at 10 mA cm⁻² and 32 mV at 50 mA cm⁻²). Remarkably, when the current density increases ($> \sim 80$ mA cm⁻²), the NF/NiCoMoO-H₂ catalyst exhibits a superior HER activity than the NF/Pt/C. It is known that the poor water dissociation of the Pt-based electrocatalysts in alkaline solutions restricts their HER performance at high current densities. However, in the NF/NiCoMoO-H₂ catalyst, the synergistic effect between Ni-Co-Mo-O nanosheets and metallic NiCo nanoparticles promotes the water dissociation on the Ni-Co-Mo-O nanosheets [37]. To our knowledge, such HER activity of NF/NiCoMoO-H₂ electrode represents the top levels among the non-precious-metal HER catalysts previously reported under alkaline conditions (Table S1).

To evaluate the HER kinetics of as-prepared catalysts, the Tafel plot was plotted based on the polarization curves through the equation $\eta = a + b \log(j)$ (a and b represent the intercept and Tafel slope, respectively.) [38,39]. As shown in Fig. 3c, The Tafel slope of NF/NiCoMoO-H₂ electrode is only 33.1 mV dec⁻¹, which is 3–4 times lower than that of NF/NiCoMoO-Ar (124 mV dec⁻¹) and pure NF (142 mV dec⁻¹). In addition, the value of 33.1 mV dec⁻¹ is highly comparable to

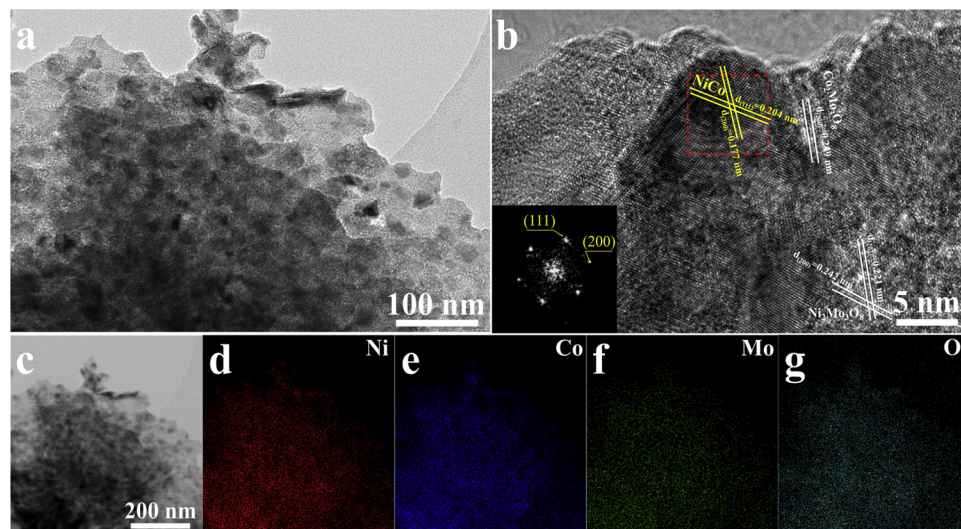


Fig. 2. The TEM characterization of NF/NiCoMoO-H₂. (a) TEM image and (b) HRTEM image (inset: the Fourier transform spectrum of the corresponding red area in HRTEM image). (c-g) STEM image and corresponding elemental mapping images of Ni, Co, Mo and O (For interpretation of the references to colour in this figure legend, the reader is referred to the web version of this article).

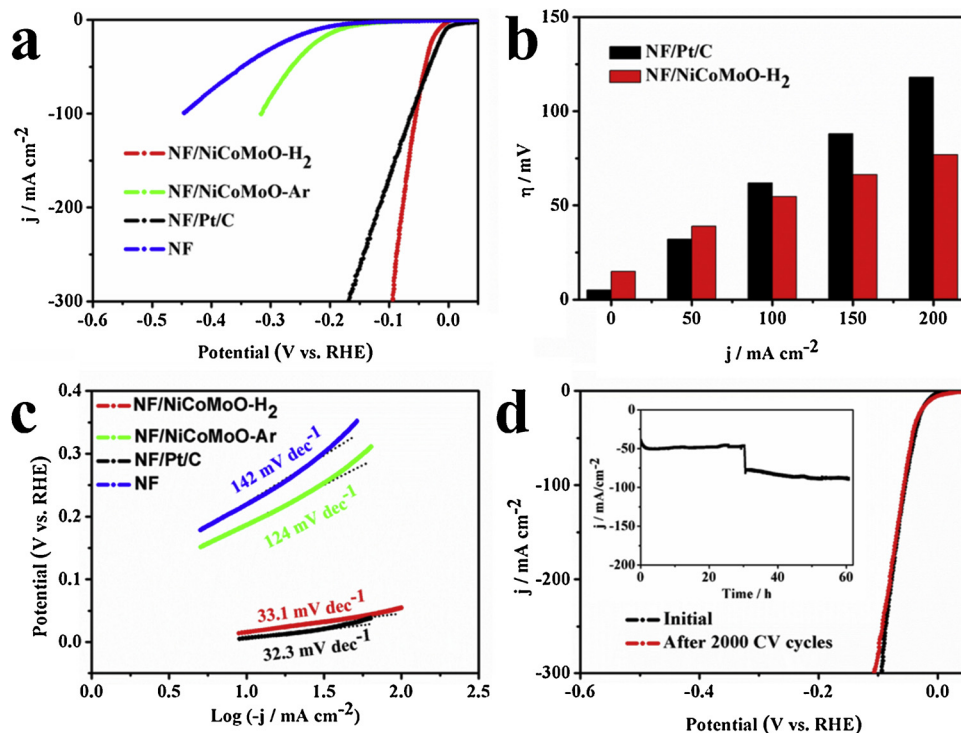


Fig. 3. Electrocatalytic performance of different catalysts. (a) Polarization curves for NF/Pt/C, NF, NF/NiCoMoO-Ar and NF/NiCoMoO-H₂. (b) Comparison of the overpotentials for the NF/NiCoMoO-H₂ and NF/Pt/C catalysts. (c) The corresponding Tafel plots. (d) Polarization curves of the NF/NiCoMoO-H₂ electrocatalyst before and after 2000 cyclic voltammetry cycles at scan rate of 100 mV s⁻¹. The inset image is long-term stability test at different potential: 83 mV vs. RHE (-1.15 V vs. SCE) and 133 mV vs. RHE (-1.2 V vs. SCE).

that of the NF/Pt/C catalyst (32.3 mV dec⁻¹). Therefore the NF/NiCoMoO-H₂ catalyst can exhibit a fast increase in the hydrogen generation rate with the applied overpotential, corresponding to the high activity presented in the polarization curves [40]. Fig. S6 shows that the exchange current densities of the different catalysts based on the extrapolation of Tafel plots. The exchange current density of the NF/NiCoMoO-H₂ electrode (4.65 mA cm⁻²) is significantly higher than those of NF/NiCoMoO-Ar (0.27 mA cm⁻²) and pure NF (0.22 mA cm⁻²), close to the value of 5.71 mA cm⁻² for NF/Pt/C, further evidencing a favorable HER reaction kinetics for the NF/NiCoMoO-H₂ electrode.

Apart from high activity, the long-term stability is also an important criterion for the evaluation of the advanced HER electrocatalysts [41]. Thus, we examined the durability of the NF/NiCoMoO-H₂ electrode using cyclic voltammetry (CV) and amperometric i-t curve methods. As shown in Fig. 3d, the increase of HER overpotential is negligible after 2000 cycles at a scan rate of 100 mV s⁻¹. In addition, the long-term stability test was successively carried out at potentials of 83 mV vs. RHE (-1.15 V vs. SCE) and 133 mV vs. RHE (-1.2 V vs. SCE) for total 60 h. The activity of the NF/NiCoMoO-H₂ catalyst is even slightly increased after 60 h of testing, indicating the excellent robustness for HER under alkaline medium.

We next investigated the chemical state of the elements in NiCoMoO-H₂ and NiCoMoO-Ar by X-ray photoelectron spectroscopy (XPS), because electrocatalytic activity is generally very sensitive to the valence and coordination environment of elements [37]. The XPS survey (Fig. S7a) shows the presence of Ni, Co, Mo and O elements in NiCoMoO-H₂. Fig. 4 shows the coexistence of high valence elements (Ni²⁺, Co²⁺ and Mo⁶⁺) and low valence elements (Ni⁰, Co⁰, Mo⁴⁺ and Mo⁵⁺) in NiCoMoO-H₂. The Ni²⁺ and Co²⁺ can efficiently weaken the O-H bond of absorbed water, facilitating the water dissociation. Meanwhile, nearby metallic NiCo nanoparticles can provide an appropriate binding energy to stabilize H adsorbed, promoting the formation of H₂ molecules. In a word, Ni-Co-Mo-O nanosheets and metallic NiCo nanoparticles in NiCoMoO-H₂ create a synergistic effect. The promoted water dissociation on the Ni-Co-Mo-O nanosheets and the stable H adsorption and transition to H₂ molecules on the metallic NiCo nanoparticles allow the catalyst to achieve excellent HER. The schematic diagrams in Fig. 4d and e illustrate the synergistic effect. This

synergistic effect is further confirmed by the experimentally measured superior HER activity of NiCoMoO-H₂ as compared to NF/NiCoMoO-Ar and the calcined NF/NiCoMoO-H₂ in air at 300 °C for 2 h (Fig. S8). In addition, Mo element also plays an important role in the HER of NiCoMoO-H₂ (Fig. 4c), where Mo⁴⁺ and Mo⁵⁺ has been proven to promote the desorption of the generated H₂ [42–45]. Meanwhile, the O 1s XPS spectra shows that the H₂ treatment increased oxygen vacancies in the catalyst, which benefit the improvement of HER activity (Fig. S7b) [46,47].

We also optimized the NF/NiCoMoO-H₂ catalyst through different annealing temperatures (400, 500 and 600 °C) in H₂/Ar atmosphere (Fig. S9). The catalyst obtained at 500 °C achieves the best HER activity (500 °C is used as the annealing temperature for the preparation of the optimum catalyst). To further evaluate the hydrogen production efficiency of NF/NiCoMoO-H₂, the Faradaic efficiency was also tested (Fig. S10), and a nearly 100% Faradaic efficiency for HER in 1 M KOH aqueous solution was achieved.

In order to further explore the origin of the excellent HER activity of the NF/NiCoMoO-H₂ catalyst, we estimated the electrical double-layer capacitance (C_{dl}) and the electrochemically active surface area (ECSA) of different samples, respectively [48,49]. As shown in Fig. S11, the C_{dl} of the NF/NiCoMoO-H₂ electrode is 98.2 mF cm⁻², which is significantly higher than the C_{dl} of NF/NiCoMoO-Ar (2.8 mF cm⁻²) and pure NF (1.1 mF cm⁻²). In addition, the ECSA of the NF/NiCoMoO-H₂ (2455 cm²) calculated from the C_{dl} is also much larger than NF/NiCoMoO-Ar (70 cm²) and pure NF (27.5 cm²). Therefore, compared to NF/NiCoMoO-Ar and pure NF, the NF/NiCoMoO-H₂ electrocatalyst has more available active sites. Furthermore, we also examined electrochemical impedance spectroscopy (EIS) to give insight into the electrode kinetics. The Nyquist plots in Fig. S12 show that the NF/NiCoMoO-H₂ electrode exhibit the smallest semicircular diameter and R_{ct}, indicating its much faster charge transfer and higher efficient HER kinetics [50]. The faster charge-transfer kinetics is deeply related to the improved conductivity of the NF/NiCoMoO-H₂ due to the increase of oxygen vacancies and the present of NiCo alloy after the hydrogenation process [47].

Inspired by such excellent HER performance, we therefore assembled a water-alkali electrolyzer using NF/NiCoMoO-H₂ as cathode

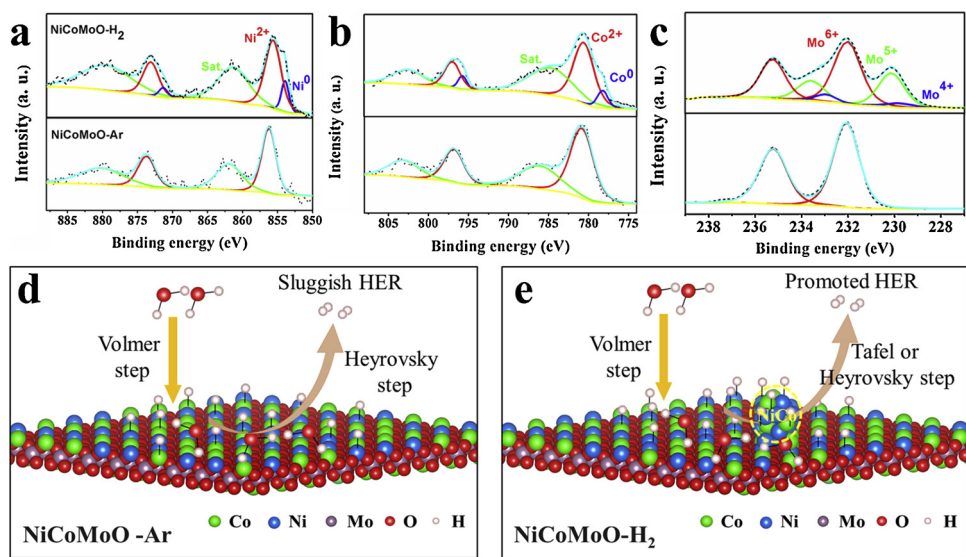
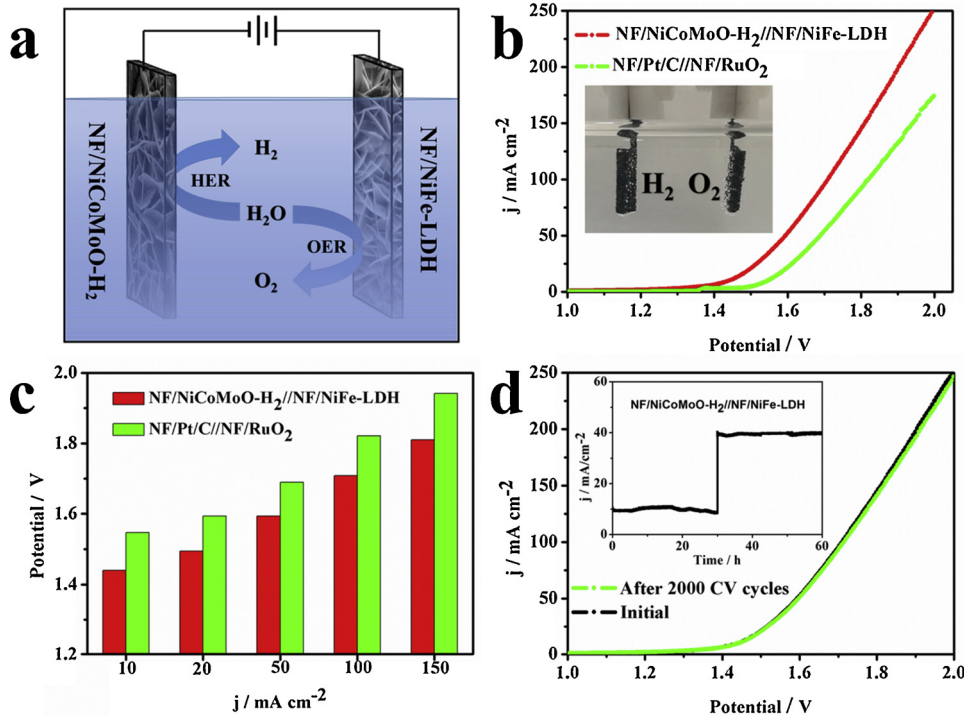


Fig. 4. High-resolution XPS spectra for NiCoMoO-H₂ and NiCoMoO-Ar. (a) Ni 2p, (b) Co 2p and (c) Mo 3d. Schematic illustration of water adsorption, water dissociation and hydrogen generation processes on (d) NiCoMoO-Ar and (e) NiCoMoO-H₂.



and NF/NiFe-LDH (NiFe-layered double hydroxide grown on NF, for details, see the Experimental Section and Fig. S13) as anode to evaluate its potential for overall water splitting in 1 M KOH aqueous solution (Fig. 5a). Fig. 5b shows that the NF/NiCoMoO-H₂/NF/NiFe-LDH has great advantages for overall water splitting, compared to NF/Pt/C//NF/RuO₂. H₂ and O₂ bubbles on the corresponding electrodes can be clearly seen (Inset in Fig. 5b). At the current densities of 10, 50 and 100 mA cm⁻², the cell voltages of NF/NiCoMoO-H₂/NF/NiFe-LDH for overall water splitting are 1.44, 1.59 and 1.71 V, respectively, which are significantly lower than those of NF/Pt/C//NF/RuO₂ (Fig. 5c). Such small cell voltage for overall water splitting is impressive and superior compared to the recently reported values of state-of-the-art materials (Table S2). Interesting, after 2000 cyclic voltammetry cycles at a scan rate of 100 mV s⁻¹ or a total 60 h continuous stability test under different cell voltages, our home-made water electrolyzer still maintained

Fig. 5. Performance characterization of water electrolysis. (a) The schematic of water electrolyzer using NF/NiCoMoO-H₂ as cathode and NF/NiFe-LDH as anode. (b) Comparison of the polarization curves of NF/NiCoMoO-H₂/NF/NiFe-LDH and NF/Pt/C//NF/RuO₂ (The mass loading of Pt/C and RuO₂ is 2.7 mg cm⁻²). Inset is a photograph showing H₂ bubbles on NF/NiCoMoO-H₂ and O₂ bubbles on NF/NiFe-LDH. (c) Comparison of the cell voltage. (d) Polarization curves of water electrolysis before and after 2000 cyclic voltammetry cycles at a scan rate of 100 mV s⁻¹. Inset is long-term stability tests of water electrolysis under 1.5 V and 1.6 V.

a robust performance for overall water splitting, demonstrating the excellent stability (Fig. 5d). Moreover, the SEM images in Fig. S14 indicated that there was no obvious destroy of the microstructure of the catalysts after long-term stability test, further evidencing the durability of the NF/NiCoMoO-H₂ catalyst.

4. Conclusion

In summary, we reported porous Ni-Co-Mo-O nanosheets decorated with NiCo nanoparticles supported on nickel foam (NF) (NF/NiCoMoO-H₂) as high efficient HER electrocatalyst in alkaline media, which was synthesized by simple hydrothermal method and annealing in H₂/Ar atmosphere. Owing to the synergistic effect between Ni-Co-Mo-O nanosheets and metallic NiCo on the improvements of H₂O dissociation, H adsorption and H₂ formation, the NF/NiCoMoO-H₂ exhibited high HER

performance and excellent stability in alkaline solution. Furthermore, the home-made water-alkali electrolyzer using NF/NiCoMoO-H₂ as cathode and NF/NiFe-LDH as anode achieved a small cell voltage of 1.44 V at 10 mA cm⁻² and performed excellent durability. The impressive results indicated that the earth-abundant and low-cost nickel-cobalt-molybdenum-oxygen based catalyst is promising for future hydrogen economy.

Declaration of Competing Interest

None.

Acknowledgements

The authors acknowledge the financial support by the Natural Science Foundation of Tianjin (No. 18JCYBJC17600). Project supported by Key Laboratory of Advanced Ceramics and Machining Technology, Ministry of Education (Tianjin University).

Appendix A. Supplementary data

Supplementary material related to this article can be found, in the online version, at doi:<https://doi.org/10.1016/j.apcatb.2019.117953>.

References

- [1] Y. Zheng, Y. Jiao, Y. Zhu, L.H. Li, Y. Han, Y. Chen, A. Du, M. Jaroniec, S.Z. Qiao, Hydrogen evolution by a metal-free electrocatalyst, *Nat. Commun.* 5 (2014) 3783.
- [2] Z. Chen, R. Wu, Y. Liu, Y. Ha, Y. Guo, D. Sun, M. Liu, F. Fang, Ultrafine Co nanoparticles encapsulated in carbon-nanotubes-Grafted graphene sheets as advanced electrocatalysts for the hydrogen evolution reaction, *Adv. Mater.* (2018) e1802011.
- [3] R. Subbaraman, D. Tripkovic, K.C. Chang, D. Strmcnik, A.P. Paulikas, P. Hirunsit, M. Chan, J. Greeley, V. Stamenkovic, N.M. Markovic, Trends in activity for the water electrolyser reactions on 3d M(Ni,Co,Fe,Mn) hydr(oxy)oxide catalysts, *Nat. Mater.* 11 (2012) 550–557.
- [4] J. McAllister, N.A. Bandeira, J.C. McGlynn, A.Y. Ganin, Y.-F. Song, C. Bo, H.N. Miras, Tuning and mechanistic insights of metal chalcogenide molecular catalysts for the hydrogen-evolution reaction, *Nat. Commun.* 10 (2019) 370.
- [5] Y.C. Chen, A.Y. Lu, P. Lu, X. Yang, C.M. Jiang, M. Mariano, B. Kaehr, O. Lin, A. Taylor, I.D. Sharp, L.J. Li, S.S. Chou, V. Tung, Structurally deformed MoS₂ for electrochemically stable, thermally resistant, and highly efficient hydrogen evolution reaction, *Adv. Mater.* 29 (2017) 1703863.
- [6] E. Hu, Y. Feng, J. Nai, D. Zhao, Y. Hu, X.W. Lou, Construction of hierarchical Ni-Co-P hollow nanobricks with oriented nanosheets for efficient overall water splitting, *Energy Environ. Sci.* 11 (2018) 872–880.
- [7] J. Wang, W. Cui, Q. Liu, Z. Xing, A.M. Asiri, X. Sun, Recent progress in cobalt-based heterogeneous catalysts for electrochemical water splitting, *Adv. Mater.* 28 (2016) 215–230.
- [8] L. Ji, P. Yan, C. Zhu, C. Ma, W. Wu, C. Wei, Y. Shen, S. Chu, J. Wang, Y. Du, J. Chen, X. Yang, Q. Xu, One-pot synthesis of porous 1T-phase MoS₂ integrated with single-atom Cu doping for enhancing electrocatalytic hydrogen evolution reaction, *Appl. Catal. B: Environ.* 251 (2019) 87–93.
- [9] Z.-Y. Wu, W.-B. Ji, B.-C. Hu, H.-W. Liang, X.-X. Xu, Z.-L. Yu, B.-Y. Li, S.-H. Yu, Partially oxidized Ni nanoparticles supported on Ni-N co-doped carbon nanofibers as bifunctional electrocatalysts for overall water splitting, *Nano Energy* 51 (2018) 286–293.
- [10] J. Chen, J. Liu, J.-Q. Xie, H. Ye, X.-Z. Fu, R. Sun, C.-P. Wong, Co-Fe-P nanotubes electrocatalysts derived from metal-organic frameworks for efficient hydrogen evolution reaction under wide pH range, *Nano Energy* 56 (2019) 225–233.
- [11] L. Tian, X. Yan, X. Chen, Electrochemical activity of Iron phosphide nanoparticles in hydrogen evolution reaction, *ACS Cataly.* 6 (2016) 5441–5448.
- [12] L. Tian, X. Yan, X. Chen, L. Liu, X. Chen, One-pot, large-scale, simple synthesis of Co₃P nanocatalysts for electrochemical hydrogen evolution, *J. Mater. Chem. A Mater. Energy Sustain.* 4 (2016) 13011–13016.
- [13] Y. Jin, H. Wang, J. Li, X. Yue, Y. Han, P.K. Shen, Y. Cui, Porous MoO₂ nanosheets as non-noble bifunctional electrocatalysts for overall water splitting, *Adv. Mater.* 28 (2016) 3785–3790.
- [14] R. Zhang, X. Wang, S. Yu, T. Wen, X. Zhu, F. Yang, X. Sun, X. Wang, W. Hu, Ternary NiCo₂P_x nanowires as pH-Universal electrocatalysts for highly efficient hydrogen evolution reaction, *Adv. Mater.* 29 (2017) 1605502.
- [15] X. Yan, L. Tian, J. Murowchick, X. Chen, Partially amorphized MnMoO₄ for highly efficient energy storage and the hydrogen evolution reaction, *J. Mater. Chem. A Mater. Energy Sustain.* 4 (2016) 3683–3688.
- [16] Z. Zhao, H. Liu, W. Gao, W. Xue, Z. Liu, J. Huang, X. Pan, Y. Huang, Surface-engineered PtNi-O nanostructure with record-high performance for electrocatalytic hydrogen evolution reaction, *J. Am. Chem. Soc.* 140 (2018) 9046–9050.
- [17] Y.F. Xu, M.R. Gao, Y.R. Zheng, J. Jiang, S.H. Yu, Nickel/nickel (II) oxide nanoparticles anchored onto cobalt (IV) diselenide nanobelts for the electrochemical production of hydrogen, *Angew. Chem. Int. Ed.* 52 (2013) 8546–8550.
- [18] X. Yan, L. Tian, M. He, X. Chen, Three-dimensional Crystalline/Amorphous Co/Co₃O₄ Core/Shell nanosheets as efficient electrocatalysts for the hydrogen evolution reaction, *Nano Lett.* 15 (2015) 6015–6021.
- [19] Y. Zheng, Y. Jiao, Y. Zhu, L.H. Li, Y. Han, Y. Chen, M. Jaroniec, S.Z. Qiao, High electrocatalytic hydrogen evolution activity of an anomalous ruthenium catalyst, *J. Am. Chem. Soc.* 138 (2016) 16174–16181.
- [20] M. Zang, N. Xu, G. Cao, Z. Chen, J. Cui, L. Gan, H. Dai, X. Yang, P. Wang, Cobalt molybdenum oxide derived high-performance electrocatalyst for the hydrogen evolution reaction, *ACS Cataly.* 8 (2018) 5062–5069.
- [21] J. Zhang, T. Wang, P. Liu, Z. Liao, S. Liu, X. Zhuang, M. Chen, E. Zschech, X. Feng, Efficient hydrogen production on MoNi₄ electrocatalysts with fast water dissociation kinetics, *Nat. Commun.* 8 (2017) 15437.
- [22] Y. Men, P. Li, J. Zhou, G. Cheng, S. Chen, W. Luo, Tailoring the electronic structure of Co₂P by N doping for boosting hydrogen evolution reaction at all pH values, *ACS Cataly.* 9 (2019) 3744–3752.
- [23] J. Zhang, T. Wang, D. Pohl, B. Rellinghaus, R. Dong, S. Liu, X. Zhuang, X. Feng, Interface Engineering of MoS₂/Ni₃S₂Heterostructures for Highly Enhanced Electrochemical Overall-Water-Splitting Activity, *Angew. Chem. Int. Ed.* 128 (2016) 6814–6819.
- [24] R. Subbaraman, D. Tripkovic, D. Strmcnik, K.-C. Chang, M. Uchimura, A.P. Paulikas, V. Stamenkovic, N.M. Markovic, Enhancing hydrogen evolution activity in water splitting by tailoring Li⁺-Ni(OH)₂-Pt interfaces, *Science* 334 (2011) 1256–1260.
- [25] J. Greeley, T.F. Jaramillo, J. Bonde, I. Chorkendorff, J.K. Nørskov, Computational high-throughput screening of electrocatalytic materials for hydrogen evolution, *Materials For Sustainable Energy: A Collection of Peer-Reviewed Research and Review Articles* from Nature Publishing Group, *World Sci.* (2011) 280–284.
- [26] X. Yan, L. Tian, X. Chen, Crystalline/amorphous Ni/NiO core/shell nanosheets as highly active electrocatalysts for hydrogen evolution reaction, *J. Power Sources* 300 (2015) 336–343.
- [27] M. Gong, W. Zhou, M.J. Kenney, R. Kapusta, S. Cowley, Y. Wu, B. Lu, M.C. Lin, D.Y. Wang, J. Yang, B.J. Hwang, H. Dai, Blending Cr₂O₃ into a Ni-O-Ni electrocatalyst for sustained water splitting, *Angew. Chem. Int. Ed.* 54 (2015) 11989–11993.
- [28] L. Peng, X. Zheng, L. Li, L. Zhang, N. Yang, K. Xiong, H. Chen, J. Li, Z. Wei, Chimney effect of the interface in metal oxide/metal composite catalysts on the hydrogen evolution reaction, *Appl. Catal. B* 245 (2019) 122–129.
- [29] M. Gong, W. Zhou, M.-C. Tsai, J. Zhou, M. Guan, M.-C. Lin, B. Zhang, Y. Hu, D.-Y. Wang, J. Yang, Nanoscale nickel oxide/nickel heterostructures for active hydrogen evolution electrocatalysis, *Nat. Commun.* 5 (2014) 4695.
- [30] X. Yan, L. Tian, K. Li, S. Atkins, H. Zhao, J. Murowchick, L. Liu, X. Chen, FeNi₃/NiFe₂O₄ nanohybrids as highly efficient bifunctional electrocatalysts for overall water splitting, *Adv. Mater. Interfaces* 3 (2016) 1600368.
- [31] C. Fan, D. Piron, P. Paradis, Hydrogen evolution on electrodeposited nickel-cobalt-molybdenum in alkaline water electrolysis, *Electrochim. Acta* 39 (1994) 2715–2722.
- [32] J. Hou, Y. Wu, S. Cao, Y. Sun, L. Sun, Active sites intercalated ultrathin carbon sheath on nanowire arrays as integrated core-shell architecture: highly efficient and durable electrocatalysts for overall water splitting, *Small* 13 (2017) 1702018.
- [33] L. Tian, J. Murowchick, X. Chen, Improving the activity of Co₃P nanoparticles for the electrochemical hydrogen evolution by hydrogenation, *Sustain. Energy Fuels* 1 (2017) 62–68.
- [34] L.Q. Mai, F. Yang, Y.L. Zhao, X. Xu, L. Xu, Y.Z. Luo, Hierarchical MnMoO₄/CoMoO₄ heterostructured nanowires with enhanced supercapacitor performance, *Nat. Commun.* 2 (2011) 381.
- [35] C. Chen, D. Yan, X. Luo, W. Gao, G. Huang, Z. Han, Y. Zeng, Z. Zhu, Construction of core-shell NiMoO₄@Ni-Co-S nanorods as advanced electrodes for high-performance asymmetric supercapacitors, *ACS Appl. Mater. Interfaces* 10 (2018) 4662–4671.
- [36] Y. Tan, H. Wang, P. Liu, C. Cheng, F. Zhu, A. Hirata, M. Chen, 3D nanoporous metal phosphides toward high-efficiency electrochemical hydrogen production, *Adv. Mater.* 28 (2016) 2951–2955.
- [37] Z.-Y. Yu, C.-C. Lang, M.-R. Gao, Y. Chen, Q.-Q. Fu, Y. Duan, S.-H. Yu, Ni-Mo-O nanorod-derived composite catalysts for efficient alkaline water-to-hydrogen conversion via urea electrolysis, *Energy Environ. Sci.* 11 (2018) 1890–1897.
- [38] K. Jiang, B. Liu, M. Luo, S. Ning, M. Peng, Y. Zhao, Y.-R. Lu, T.-S. Chan, F.M. de Groot, Y. Tan, Single platinum atoms embedded in nanoporous cobalt selenide as electrocatalyst for accelerating hydrogen evolution reaction, *Nat. Commun.* 10 (2019) 1743.
- [39] X. Yan, K. Li, L. Lyu, F. Song, J. He, D. Niu, L. Liu, X. Hu, X. Chen, From water oxidation to reduction: transformation from Ni_xCo_{3-x}O₄ nanowires to NiCo/NiCo_x heterostructures, *ACS Appl. Mater. Interfaces* 8 (2016) 3208–3214.
- [40] Y. Yang, K. Zhang, H. Lin, X. Li, H.C. Chan, L. Yang, Q. Gao, MoS₂-Ni₃S₂ heteronanorods as efficient and stable bifunctional electrocatalysts for overall water splitting, *ACS Cataly.* 7 (2017) 2357–2366.
- [41] I.S. Amiuu, Z. Pu, X. Liu, K.A. Owusu, H.G.R. Monestel, F.O. Boakye, H. Zhang, S. Mu, Multifunctional Mo-N/C@MoS₂ electrocatalysts for HER, OER, ORR, and Zn-Air batteries, *Adv. Funct. Mater.* 27 (2017) 1702300.
- [42] D.R. Cummins, U. Martinez, A. Sherehiy, R. Kappera, A. Martinez-Garcia, R.K. Schulze, J. Jasinski, J. Zhang, R.K. Gupta, J. Lou, Efficient hydrogen evolution in transition metal dichalcogenides via a simple one-step hydrazine reaction, *Nat. Commun.* 7 (2016) 11857.
- [43] Y.J. Tang, M.R. Gao, C.H. Liu, S.L. Li, H.L. Jiang, Y.Q. Lan, M. Han, S.H. Yu, Porous molybdenum-based hybrid catalysts for highly efficient hydrogen evolution, *Angew. Chem. Int. Ed.* 54 (2015) 12928–12932.
- [44] S. Hao, L. Chen, C. Yu, B. Yang, Z. Li, Y. Hou, L. Lei, X. Zhang, NiCoMo hydroxide

nanosheet arrays synthesized via chloride corrosion for overall water splitting, *ACS Energy Lett.* 4 (2019) 952–959.

[45] L. Yang, L. Zeng, H. Liu, Y. Deng, Z. Zhou, J. Yu, H. Liu, W. Zhou, Hierarchical microsphere of MoNi porous nanosheets as electrocatalyst and cocatalyst for hydrogen evolution reaction, *Appl. Catal. B: Environ.* 249 (2019) 98–105.

[46] Z. Xiao, Y. Wang, Y.-C. Huang, Z. Wei, C.-L. Dong, J. Ma, S. Shen, Y. Li, S. Wang, Filling the oxygen vacancies in Co_3O_4 with phosphorus: an ultra-efficient electrocatalyst for overall water splitting, *Energy Environ. Sci.* 10 (2017) 2563–2569.

[47] X. Yan, L. Tian, X. Tan, M. Zhou, L. Liu, X. Chen, Modifying oxide nanomaterials' properties by hydrogenation, *MRS Commun.* 6 (2016) 192–203.

[48] Y.Y. Chen, Y. Zhang, X. Zhang, T. Tang, H. Luo, S. Niu, Z.H. Dai, L.J. Wan, J.S. Hu, Self-templated fabrication of $\text{MoNi}_{4-x}/\text{MoO}_{3-x}$ nanorod arrays with dual active components for highly efficient hydrogen evolution, *Adv. Mater.* 29 (2017) 1703311.

[49] X. Yan, L. Tian, S. Atkins, Y. Liu, J. Murowchick, X. Chen, Converting CoMoO_4 into CoO/MoO_x for overall water splitting by hydrogenation, *ACS Sustain. Chem. Eng.* 4 (2016) 3743–3749.

[50] K.N. Dinh, P. Zheng, Z. Dai, Y. Zhang, R. Dangol, Y. Zheng, B. Li, Y. Zong, Q. Yan, Ultrathin porous NiFeV ternary layer hydroxide nanosheets as a highly efficient bifunctional electrocatalyst for overall water splitting, *Small* 14 (2017) 1703257.